



Effects of 20–100 nm particles on liquid clouds in the clean summertime Arctic

W. Richard Leitch¹, Alexei Korolev¹, Amir A. Aliabadi^{1,a}, Julia Burkart², Megan D. Willis², Jonathan P. D. Abbatt², Heiko Bozem³, Peter Hoor³, Franziska Köllner⁴, Johannes Schneider⁴, Andreas Herber⁵, Christian Konrad⁵, and Ralf Brauner⁶

¹Environment and Climate Change Canada, Toronto, Canada

²Department of Chemistry, University of Toronto, Toronto, Canada

³Institute for Atmospheric Physics, University of Mainz, Mainz, Germany

⁴Particle Chemistry Department, Max Planck Institute for Chemistry, Mainz, Germany

⁵Alfred Wegener Institute Helmholtz Centre for Polar and Marine Research, Bremerhaven, Germany

⁶Department of Maritime and Logistics Studies, Jade University, Elsfleth, Germany

^anow at: Environmental Engineering, University of Guelph, Guelph, Canada

Correspondence to: W. Richard Leitch (richard.leitch@canada.ca)

Received: 10 December 2015 – Published in Atmos. Chem. Phys. Discuss.: 29 January 2016

Revised: 28 July 2016 – Accepted: 1 August 2016 – Published: 8 September 2016

Abstract. Observations addressing effects of aerosol particles on summertime Arctic clouds are limited. An airborne study, carried out during July 2014 from Resolute Bay, Nunavut, Canada, as part of the Canadian NETCARE project, provides a comprehensive in situ look into some effects of aerosol particles on liquid clouds in the clean environment of the Arctic summer. Median cloud droplet number concentrations (CDNC) from 62 cloud samples are 10 cm^{-3} for low-altitude cloud (clouds topped below 200 m) and 101 cm^{-3} for higher-altitude cloud (clouds based above 200 m). The lower activation size of aerosol particles is $\leq 50\text{ nm}$ diameter in about 40 % of the cases. Particles as small as 20 nm activated in the higher-altitude clouds consistent with higher supersaturations (S) for those clouds inferred from comparison of the CDNC with cloud condensation nucleus (CCN) measurements. Over 60 % of the low-altitude cloud samples fall into the CCN-limited regime of Mauritsen et al. (2011), within which increases in CDNC may increase liquid water and warm the surface. These first observations of that CCN-limited regime indicate a positive association of the liquid water content (LWC) and CDNC, but no association of either the CDNC or LWC with aerosol variations. Above the Mauritsen limit, where aerosol indirect cooling may result, changes in particles with diameters from 20 to 100 nm exert a relatively strong influence on the CDNC.

Within this exceedingly clean environment, as defined by low carbon monoxide and low concentrations of larger particles, the background CDNC are estimated to range between 16 and 160 cm^{-3} , where higher values are due to activation of particles $\leq 50\text{ nm}$ that likely derive from natural sources. These observations offer the first wide-ranging reference for the aerosol cloud albedo effect in the summertime Arctic.

1 Introduction

Mass concentrations of the atmospheric aerosol in the Arctic are higher during winter than in summer due to differences in transport of anthropogenic particles and wet scavenging (e.g. Barrie, 1986; Stohl, 2006). Atmospheric chemistry and aerosol cloud Arctic research has largely focussed on the springtime. The winter-to-summer transition offers the opportunity to examine changes in chemistry as the sun rises over the polluted polar atmosphere (e.g. Barrie et al., 1988) and to study impacts of anthropogenic aerosol on the Arctic solar radiation balance (e.g. Law and Stohl, 2007; Quinn et al., 2008). Greater-than-expected warming of the Arctic (e.g. Christensen et al., 2013) and rapidly diminishing Arctic sea ice extent (e.g. Maslanik et al., 2011) have drawn considerable attention to the role of anthropogenic and biomass burn-

ing (BB) particles as warming agents for the Arctic (e.g. Law and Stohl, 2007; Quinn et al., 2008; Shindell et al., 2008; Brock et al., 2011; Jacob et al., 2010; UNEP, 2011; Stohl et al., 2013). Recent evidence indicates that the net impact of aerosol particles on the Arctic over the past century has been one of cooling rather than warming (Najafi et al., 2015).

Low-level liquid water clouds are frequent in the sunlit Arctic summer (e.g. Intrieri et al., 2001), and these clouds can have a net cooling effect (e.g. Brenner et al., 2001; Garrett et al., 2004; Lubin and Vogelmann, 2010; Zhao and Garrett, 2015; Zamora et al., 2016). Knowledge of the influence of the atmospheric aerosol on climatic aspects of these clouds is complicated by the relatively large potential differences in the albedo of the underlying surface (e.g. Herman, 1977; Lubin and Vogelmann, 2010) and the fact that the Arctic is relatively free of anthropogenic influence in summer, which means that particles from natural sources can be the most significant nuclei for cloud droplets. Those sources shift the number distribution toward particles smaller than 100 nm (e.g. Heintzenberg and Leck, 1994; Ström et al., 2003; Heintzenberg et al., 2006; Engvall et al., 2008; Tunved et al., 2013; Leaitch et al., 2013; Heintzenberg et al., 2015). Particles smaller than 100 nm are often dismissed as being too small to nucleate cloud droplets due to the assumption that the cooling mechanisms are too slow to generate the supersaturation (S) required to activate the smaller particles in Arctic liquid clouds (e.g. Garrett et al., 2004; Lubin and Vogelmann, 2010; Browse et al., 2014; Zhao and Garrett, 2015). That assumption may lead to reduced estimates from natural feedbacks to climate and increased estimates of aerosol indirect forcing from anthropogenic sources. Lohmann and Leck (2005) hypothesized the need for highly surface-active particles to explain cloud condensation nucleus (CCN) activity at S less than 0.3 %. However, cloud S is also strongly constrained by the concentrations of particles larger than 100 nm, and, in the clean summertime Arctic environment with relatively low concentrations of particles larger than 100 nm, there is some evidence that higher S may be achieved and smaller particles activated (e.g. Hudson et al., 2010; Korhonen et al., 2008; Leaitch et al., 2013). Further, the suggestion that the minima between 50 and 100 nm in Arctic particle size distributions result from cloud processing implies consistent activation sizes less than 100 nm (Heintzenberg et al., 2015). The effect of the background aerosol on liquid clouds has been identified as one of the most important factors for reducing uncertainty in the aerosol cloud albedo effect (Carslaw et al., 2013). Moreover, the effectiveness of particles smaller than 100 nm for cloud droplet nucleation is a large factor in that uncertainty.

Effects of pollution on clouds may also lead to warming, but a reference to clean clouds is still required (e.g. Garrett et al., 2009). Mauritsen et al. (2011) modelled cloud radiative forcing for low clouds using CCN number concentrations derived from shipborne observations over the Arctic Ocean (Tjernström et al., 2004, 2014). They found the impact from

changes in CCN for ultra-low values ($< 10 \text{ cm}^{-3}$), where CCN concentrations are equivalent to model cloud droplet number concentration (CDNC), results in a net warming due to associated long-wave changes, whereas for concentrations greater than 10 cm^{-3} CCN increases are estimated to produce a net atmospheric cooling. This CCN concentration threshold is referred to here as the “Mauritsen limit”, although this value of 10 cm^{-3} is not a universal limit (Mauritsen et al., 2011). In the clean summertime Arctic, knowledge of the natural aerosol and its influence on cloud microphysics is critical to the assessment of aerosol effects on Arctic climate.

Past studies of Arctic aerosols and clouds have emphasized the areas of the Beaufort and Chukchi seas (e.g. Hobbs and Rango, 1998; Curry, 2001, and references therein; Lohmann et al., 2001; Yum and Hudson, 2001; Peng et al., 2002; Wylie and Hudson, 2002; Earle et al., 2011; Lance et al., 2011; Jouan et al., 2014; Klingebiel et al., 2015). Most of those studies have focused on springtime when the aerosol can be influenced by anthropogenic or BB sources. As well, there has been considerable interest in mixed-phase clouds in the lower Arctic troposphere (e.g. Shupe et al., 2004; Sandvik et al., 2007; Morrison et al., 2012), but a notable lack of in situ aerosol observations in combination with liquid water clouds over the summertime Arctic. Among the studies that have considered in situ aerosol measurements and summertime Arctic clouds, Zamora et al. (2016) examined the efficiency of BB plumes on indirect forcing. They estimated half of the possible maximum forcing from these plumes, mostly due to the reduction in cloud-base S by higher concentrations of larger particles that control water uptake. Shupe et al. (2013) discussed some differences between clouds coupled and uncoupled to the surface. They did not conduct in situ cloud microphysics observations, and their vertical aerosol characterizations were constrained to particles $> 300 \text{ nm}$. Hobbs and Rango (1998) found that droplets in low clouds in June over the Beaufort Sea occasionally contained drops as large as $35 \mu\text{m}$ diameter. They also found that cloud-top CDNC correlated significantly with cloud-base “aerosols”. They suggested that cloud-top entrainment did not control CDNC, although there may be times when entrainment influences Arctic CDNC (e.g. Klingebiel et al., 2015).

Motivated by limited knowledge of aerosol effects on summertime Arctic clouds and particle activation details, the Canadian Network on Climate and Aerosols: Addressing Key Uncertainties in Remote Canadian Environments (NETCARE – <http://www.netcare-project.ca/>) conducted airborne aerosol and cloud observations during July 2014 in the area around Resolute Bay, Nunavut, Canada. The observations from this study are used here to characterize CDNC, liquid water content (LWC) and the volume-weighted mean droplet diameter (VMD). Further, aerosol particle size distributions (5 nm and larger; cloud condensation nuclei concentrations (CCNC) at 0.6% supersaturation) from the outside of clouds

are compared with droplet number concentrations from the inside of clouds. Specifically, in the indicated sections, the following questions are addressed.

1. Given the scarcity of data, what are the characteristics of clouds in the summertime Arctic, and do clouds near the surface have characteristics different from those aloft? (Sect. 3.2)
2. What are the sizes of particles that act as nuclei for cloud droplets? Will this allow a closer connection between aerosol processes, particle sizes and climate effects? (Sect. 3.3)
3. What is the relationship between droplet size and droplet number? In particular, what is the aerosol influence on cloud below the Mauritsen limit, and is it possible to assess a background influence of the aerosol on clouds in the Arctic summer? (Sect. 3.4)

2 Methodologies

The instrument platform was the Alfred Wegener Institute (AWI) Polar 6 aircraft, a DC-3 aircraft converted to a Basler BT-67 (see Herber et al., 2008).

2.1 Instrumentation

The following measurements are relevant to this discussion:

- a. Particle number concentrations >5 nm diameter were measured with a TSI 3787 water-based ultrafine condensation particle counter (UCPC), sampling at a flow rate of 0.6 L min^{-1} . Hereafter, these measurements are referred to as N5.
- b. Aerosol particle size distributions from 20 to 100 nm (45 s up scans and 15 s down scans) were measured using a Brechtel Manufacturing Incorporated (BMI) scanning mobility system (SMS) coupled with a TSI 3010 condensation particle counter (CPC). The sheath and sample flows were set to 6 and 1 L min^{-1} . BMI software was used to process these distributions.
- c. Aerosol particle size distributions from 70 nm to $1 \mu\text{m}$ were measured using a Droplet Measurement Technology (DMT) ultra-high sensitivity aerosol spectrometer (UHSAS) that detects particles using scattering of 1054 nm laser light (e.g. Cai et al., 2008).
- d. CCNC (0.6 %) were measured using a DMT CCN model 100 counter operating behind a DMT low-pressure inlet at approximately 650 hPa. For the nominal water S of 1 %, the effective S at 650 hPa was found to be 0.6 % as discussed in the Supplement. This S was held constant throughout the study for greater measurement stability and improved response and to examine the hygroscopicity of smaller particles.

- e. Droplet size distributions from 2 to $45 \mu\text{m}$ were measured with a Particle Measuring Systems (PMS) FSSP-100. This FSSP-100 had been modified with new tips to reduce shattering artifacts (Korolev et al., 2011). It was mounted in a canister under the port-side wing. The CDNC, VMD and LWC are calculated from the measured droplet distributions.
- f. Two-dimensional cloud particle images from about 50 to $800 \mu\text{m}$ were measured using a PMS 2D-C greyscale probe. These observations are used here only to ensure the absence of the ice phase. This 2D-C probe was also modified with new tips to reduce shattering artifacts (Korolev et al., 2011). It was mounted in a canister beside the FSSP-100.
- g. Carbon monoxide (CO) is used here as a relative indicator of aerosol influenced by pollution sources and as a potential tracer for aerosol particles entering cloud. CO was measured with an Aerolaser ultra-fast CO monitor model AL 5002 based on vacuum ultraviolet fluorimetry, employing the excitation of CO at 150 nm. This instrument was modified such that in situ calibrations could be conducted in flight.

Details of the instrument calibration and evaluations are given in the Supplement (Sect. S1).

2.2 State parameters and winds

State parameters and meteorological measurements were made with an AIMMS-20, manufactured by Aventech Research Inc. This instrument consists of three modules: (1) an air data probe that measures the three-dimensional aircraft-relative flow vector (true air speed, angle-of-attack and sideslip), temperature, and relative humidity and includes a three-axis accelerometer pack for turbulence measurement; (2) an inertial measurement unit that consists of three gyros and three accelerometers providing the aircraft angular rate and acceleration; (3) a global positioning system for aircraft 3-D position and inertial velocity. Horizontal and vertical wind speeds were measured with accuracies of 0.50 and 0.75 m s^{-1} , respectively. However, the vertical resolution was insufficient to measure gusts in the sampled clouds. The accuracy and resolution for temperature measurement are 0.30 and $0.01 \text{ }^\circ\text{C}$. The accuracy and resolution for relative humidity measurement are 2.0 and 0.1 %. The sampling frequency is 1 Hz.

2.3 Inlets

Aerosol particles were sampled through a shrouded inlet diffuser (diameter 0.35 cm at intake point), which is the same inlet discussed by Leitch et al. (2010). For the airspeeds during this study, particle transmission by the inlet is near unity for particles from 20 nm to $<1 \mu\text{m}$. The intake was connected inside the cabin to a 1.9 cm OD stainless steel mani-

Table 1. Summary of averaged cloud observations with $LWC > 0.01 \text{ g m}^{-3}$ for study periods 1 and 2. Values without parentheses are referenced to ambient volumes and values in parentheses are referenced to standard atmospheric pressure and temperature (STP). 5 and 95 are the 5th and 95th percentiles.

Measurement	Period 1 (5–11 July): 35 samples; 1.2 h in cloud			Period 2 (11–21 July): 27 samples; 0.4 h in cloud		
	Mean	Median	5; 95	Mean	Median	5; 95
Altitude (m m.s.l.)	920	178	88; 2272	1011	835	97; 2608
Temperature ($^{\circ}\text{C}$)	-1.9	-0.4	-6.5; 2.2	+1.2	+2.2	-4.9; 3.5
CDNC (STP; cm^{-3})	75 (85)	93 (91)	1.1; 154 (1.1; 185)	73 (83)	52 (55)	13; 228 (14; 265)
LWC (STP; g m^{-3})	0.12 (0.13)	0.10 (0.12)	0.014; 0.32 (0.013; 0.32)	0.12 (0.13)	0.12 (0.13)	0.025; 0.26 (0.024; 0.31)
VMD(μm)	17.2	18.7	9.9; 30.0	15.0	14.5	9.1; 21.4
CCNC (0.6 %; cm^{-3}): (17 P-1; 27 P-2)	90	120	2; 168	81	43	18; 227
N50 (cm^{-3})	113	134	4.8; 319	126	68	29; 334
N100 (cm^{-3})	35	47	1.3; 73	81	31	13.8; 274
CDNC (STP)/CCNC (0.6 %)	0.75	0.56	0.18; 1.50	1.18	1.22	0.47; 1.87
CDNC (STP)/N50	0.82	0.90	0.16; 1.40	0.73	0.68	0.28; 1.08
CDNC (STP)/N100	2.78	2.63	0.28; 7.94	1.37	1.25	0.58; 2.15
CCNC (0.6 %)/N50	0.64	0.63	0.50; 0.84	0.64	0.64	0.52; 0.87
CCNC (0.6 %)/N100	1.92	1.79	0.67; 3.11	1.27	1.0	0.75; 2.28
CO (ppbv)	79	80	77; 81	90	87	81; 108
LWP (g m^{-2}); (13 P-1; 23 P-2)	30	27	1.5; 4	22	13	1.0; 70.5

fold off of which sample lines were drawn to the various instrument racks using angled inserts. Total flow at the intake point was approximately isokinetic at 55 L min^{-1} based on the sum of flows drawn by the instrumentation (35 L min^{-1}) and the measured manifold exhaust flow. The manifold exhaust flowed freely into the back of the cabin such that the intake flow varied with aircraft true airspeed and the manifold was not significantly overpressured.

CO was sampled through a separate inlet consisting of a 0.40 cm OD Teflon tube using aircraft forward motion to push air into the line in combination with a rear-facing 0.95 cm OD Teflon exhaust line that reduced the line pressure. The continuously measured sample flow was approximately 12 L min^{-1} .

2.4 Data analysis approach

Eleven research flights were conducted from Resolute Bay, Nunavut ($74^{\circ}40'48'' \text{ N}$, $94^{\circ}52'12'' \text{ W}$), from 4 to 21 July 2014, inclusive. These measurements were associated with two distinct weather regimes. During period 1 (4–12 July), weather conditions around Resolute Bay were affected by an upper low (Supplement Fig. S4). The wind speeds at 500 hPa were mostly light and variable. The surface (1000 hPa) was dominated by weak high pressure with generally clear skies, light winds and occasional scattered to broken stratocumulus. Low-cloud or fog was at times present in association with

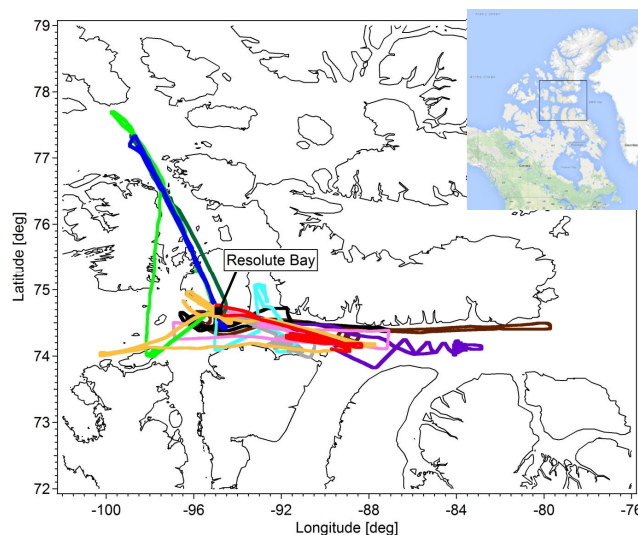


Figure 1. Compilation of the flight tracks. All flights originated from Resolute Bay ($74^{\circ}40'48'' \text{ N}$, $94^{\circ}52'12'' \text{ W}$).

open water, and the air was relatively clean, as discussed below. There was a transition period from 13 to 16 July when flights were not possible due to fog at Resolute Bay. During period 2 (17–21 July), the area came under the influence of a deep low-pressure system to the south (Fig. S5) that brought

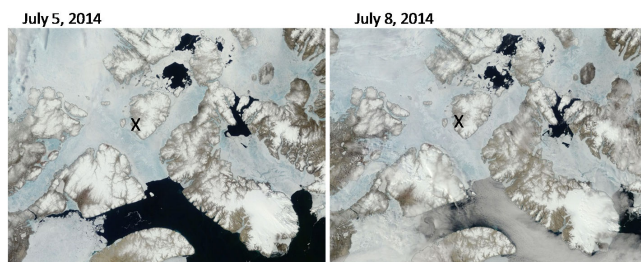


Figure 2. Satellite images from 5 July when LA clouds were sampled over the two polynyas to the north and from 8 July when LA clouds were sampled along Lancaster Sound. Lancaster Sound is cloud free on 5 July and mostly covered by cloud on 8 July. Lancaster Bay is marked with a “X”. Images are courtesy of NASA Worldview: <https://earthdata.nasa.gov/labs/worldview/>.

more wind and higher cloud. The air was not as clean as during period 1, based on the measured aerosol mass and CO concentrations (see Table 1). This was possibly due to transport of BB aerosol from the Northwest Territories; further discussion in Sect. 2.3.1. Based on the bulk Richardson number and data from radiosondes, Aliabadi et al. (2016a) estimated boundary-layer heights at 254 m (± 155 m) across the study.

A summary of all flight tracks is shown in Fig. 1. Flights mostly consisted of vertical profiles and low-level transits over ice, water and melt ponds that contributed to the formation of low cloud; low cloud is defined here as cloud tops below 200 m m.s.l. Higher-level cloud was also sampled during the profiles and transits. The polynyas that were sampled are shown in the top centre of each panel of Fig. 2. Cloud was sampled on 8 of the 11 flights, more frequently during period 1 because of overall better visual contrast between clouds and surfaces. Furthermore, period 2 was marked by the presence of the Canadian Coast Guard Ship *Amundsen* in Lancaster Sound (bottom centre of each Fig. 2 panel) when the flights were focused on sampling the ship’s plume (e.g. Aliabadi et al., 2016b).

All aerosol number concentrations are given in terms of standard atmospheric pressure and temperature (STP: 1 atm and 15 °C). The CDNC are also referenced to STP where comparisons are made with the aerosol number concentrations. Number concentrations of particles larger than 100 nm (N100) are taken from the UHSAS. All data, except the SMS, are 1 s averages that represent a sampling path length of 60–80 m. Size distributions between 20 and 100 nm are from the SMS and are 1 min averages. Except for the Fig. S3 example, all particle number concentrations smaller than 100 nm are from the SMS. N_{x-100} refers to the number concentration within the interval “ $x-100$ ” where x ranges between 20 and 90. Values of N_x with $x < 100$ are derived from the sum of N_{x-100} (SMS) + N100 (UHSAS).

Clouds were sampled during a flight whenever possible, mostly by ascending or descending through them. It was not

possible to sample below the low-altitude (LA) cloud bases. Most clouds were liquid phase, based on the 2D-C grey images of cloud particles $> 50 \mu\text{m}$, and only liquid-phase clouds are discussed here. In addition, none of the liquid clouds exhibited detectable precipitation, except that droplets in a couple of the lowest-altitude clouds were very low in number and relatively large in size (30–40 μm); considering the settling speeds of such droplets, they may be viewed as precipitating. The higher-altitude (HA) clouds were either stratus or stratocumulus, whereas the low-level clouds were fog or stratus. Although still light, turbulence appeared to be the greatest in the 7 July stratocumulus. Cloud droplet sizes are represented by the VMD, which has the property that the VMD can be used with CDNC to calculate LWC.

The pre-cloud aerosol for the HA clouds is mostly derived from averages of values collected within about 50 m of cloud base when a cloud base was visible and achievable. In some cases, as discussed in Sects. 2.4.1 and 2.4.2, the pre-cloud aerosol concentrations include contributions from above cloud (19 July) or are from similar or lower altitudes in the clear air upwind of the cloud. For the aerosol measurements made with the 1 min averaged number concentrations from the SMS, values from further below cloud are necessary in some cases. These values are, however, consistent with the 1 s aerosol measurements closer to cloud base.

Every possible liquid cloud was sampled along a flight path, and some cloud layers were sampled more than once. That will bias the sample numbers to clouds of greater spatial extent. However, that bias is appropriate from a climate perspective since cloud extent is a major factor for the impacts of clouds on climate. A total of 62 liquid water cloud samples, or averages of individual cloud penetrations, were averaged with the constraint that the mean LWC is $> 0.01 \text{ g m}^{-3}$. The samples are integrations over periods ranging from 11 to 1000 s with a median sample time of 65 s that is equivalent to a horizontal path length of about 4 km.

In Sects. 2.4.1 and 2.4.2, a range of detailed examples are used to show how the aerosol observations relate to the cloud observations for the HA cloud (clouds based above 200 m) and LA cloud (clouds topped below 200 m), to (1) demonstrate how the pre-cloud aerosol concentrations were assessed for the 62 samples and to (2) note where effects of entrainment may be a factor and how multiple cloud layers are considered. At 200 m or below, the LA clouds were in the boundary layer, in flight indistinguishable from the surface (i.e. some were possibly fog). Thus, sampling below such clouds was not possible due to proximity to the surface. Besides cloud microphysics, the only in-cloud measurements considered valid are the CO and thermodynamics. For completeness, the aerosol measurements within cloud are included in the plots associated with Sects. 2.4.1 and 2.4.2, but such measurements, including the CCN, are unreliable due to issues of drying and partial drying associated with the inlet and a particular instrument as well as droplet shattering on the inlet (e.g. Hudson and Frisbie, 1991, and Hallett and

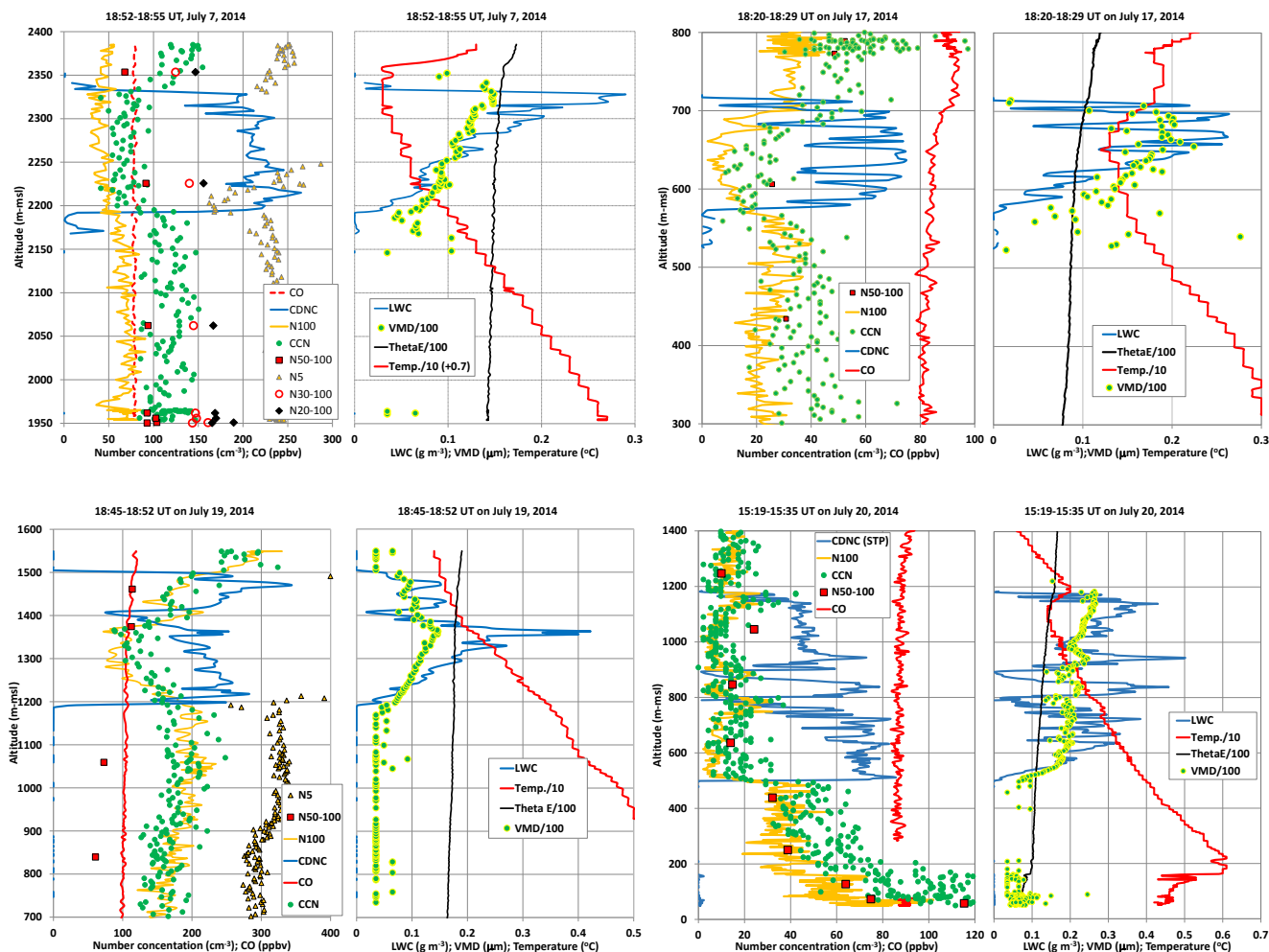


Figure 3. Four examples of profiles through higher-altitude clouds. **(a)** Case from 7 July showing CO, CDNC, CCNC (0.6 %) and particle number concentrations, where N_x -100, N100 and N5 are for particles sized between “ x ” and 100 nm, > 100 and > 5 nm, respectively. **(b)** Case from 7 July showing LWC, VMD, θ_e and temperature, where VMD, θ_e and temperature have been scaled as indicated in the legend. **(c)** As in **(a)** but for the case from 17 July and without N5. **(d)** As in **(b)** but for the case from 17 July. **(e)** As in **(a)** but for the case from 19 July. **(f)** As in **(b)** but for the case from 19 July. **(g)** As in **(a)** but for the case from 20 July and without N5. **(h)** as in **(b)** for the but case from 20 July. The CDNC are all referenced to standard atmospheric pressure and temperature (STP), and θ_e is given in degrees Centigrade before scaling.

Christensen, 1984). The in-cloud aerosol measurements are not part of the subsequent analysis.

2.4.1 Higher-altitude cloud examples

Four examples of profiles through HA clouds are shown in Fig. 3. There are two panels for each profile: the left-hand panel shows CO, CDNC and particle number concentrations (N5, N_x -100, N100, CCNC (0.6 %)); the right-hand panel shows temperature, equivalent potential temperature (θ_e), LWC and VMD. The temperatures, θ_e and VMD are scaled as indicated.

7 July case (Fig. 3a, b)

One of several similar profiles through a stratocumulus layer during the transits to and from the polynyas north of Resolute Bay. The CDNC (at STP) are relatively constant with altitude while LWC and VMD both increase steadily with altitude. These features characterize cloud formation by lifting of air, and they indicate that the cloud droplets were nucleated on particles from below cloud base. The cloud top is relatively sharply capped by a temperature inversion of about 2 °C at 2350 m, and the particle profiles along with θ_e and CO are relatively constant below cloud base. There is no indication that entrainment, based on the LWC profile, does anything other than reduce the CDNC. Within cloud,

the number concentrations of larger particles (N100) is reduced due to nucleation scavenging, although such particles are not completely eliminated as smaller droplets can enter the inlet and dry in the sampling lines. Smaller particles can be artificially increased in cloud due to the shattering of larger droplets on the aerosol intake (e.g. Hudson, 1993), as indicated by the increase in the corresponding N5 higher in cloud. Thus, in-cloud aerosol measurements are shown here only for completeness, but they are not used in the subsequent analysis. CDNC range up to 265 cm^{-3} and the mean value is 199 cm^{-3} . Below cloud base, the N5, N20-100, N30-100, N50-100, N100 and CCNC (0.6 %) are approximately 235, 167, 145, 94, 67 and 117 cm^{-3} , respectively. The below-cloud N20 of 234 cm^{-3} approximately equals the N5, offering confidence in terms of number concentration closure. The N30 (N30-100 + N100) compares most closely with the mean CDNC, leading to the conclusion that on average cloud droplets nucleated on particles down to about 30 nm. Based on the maximum CDNC, it is possible that particles as small as 20 nm contributed to the CDNC in this cloud; for 20 nm particles of ammonium sulfate to activate, Köhler equilibrium theory indicates that S in the cloud bases would have had to reach above 1.5 %.

17 July case (Fig. 3c, d)

The maximum and mean CDNC (STP) of about 75 and 55 cm^{-3} , respectively, are lower while the VMD peak of $20\text{ }\mu\text{m}$ is higher compared with the 7 July profile. The LWC are generally similar between 7 and 17 July except that there are more breaks in the 17 July profile. Many of those breaks are due to the aircraft passing through the edges of cloud during this profile. The inversion topping the cloud is weaker and the LWC peak occurs further from cloud top in the 17 July case than the 7 July case. That LWC feature in combination with the general CO increase, beginning at about 660 m, suggests that the erosion of cloud top by entrainment went deeper into the 17 July cloud. Above 660 m, the CDNC also decrease, suggesting the higher concentrations of N50-100, N100 and CCN above cloud relative to below cloud did not enhance the CDNC. Continuity from at least 100 m below cloud base is indicated by the CO and θ_e profiles, and the N50 approximates the mean CDNC and possibly maximum CDNC. The CCNC (0.6 %) are $30\text{--}40\text{ cm}^{-3}$ below cloud, indicating a S higher than 0.6 %. The comparison between the 7 and 17 July cases is a specific example of the potential importance of smaller particles for the cloud albedo effect.

19 July case (Fig. 3e, f)

The July 19 profile includes two cloud layers, one from 1200 to 1400 m and a second from 1400 to 1500 m. The layer separation appears in the CO concentrations, which are approximately uniform through the lower layer and increasing in the upper layer. The CO levels of 100+ ppbv in this case

are among the highest observed during this study. Transport patterns suggest that BB contributed to this aerosol (Köllner et al., 2015). The mean CDNC (STP) in the lower and upper layers are 239 and 276 cm^{-3} , respectively. The VMD reached $15\text{ }\mu\text{m}$ in the lower layer. The VMDs are overall smaller and decrease with altitude in the upper layer, corresponding to the lower LWC and higher CDNC. In the upper layer, the CDNC increase from cloud bottom to near cloud top consistent with the increase in aerosol from below the layer to above the layer. The N50 and N100 estimated for the lower (upper) layer are 269 (334) and 197 (221) cm^{-3} , respectively, where the upper layer values are an average of the aerosol at 1400 m and just above cloud top. Thus, on average the CDNC in both layers are approximated by activation of particles sized between 50 and 100 nm, and the maximum CDNC are approximated by activation of 50 nm particles. The CCNC (0.6 %) are slightly below the N100, which would be consistent with the lower hygroscopicity of BB particles. Comparison of below-cloud CCNC (0.6 %) with CDNC suggests cloud S above 0.6 %.

20 July case (Fig. 3g and h)

This is a more complex cloud with substantial LWC variations that suggest three cloud layers. The values of mean CDNC at STP are 45, 49 and 65 cm^{-3} in the upper, middle and lower layers, respectively. The VMDs reach about $20\text{ }\mu\text{m}$ in the lower layer and $26\text{ }\mu\text{m}$ in the upper layer with the lower CDNC. These layers are relatively stable with CO and θ_e increasing slightly from below the cloud to above the top cloud layer. N50 just below the lower layer approximately equals CDNC in that layer. It is more difficult to estimate the pre-cloud aerosol for the middle and upper layers, but particles at least as small as 50 nm were apparently activated. For the summary statistics, the respective pre-cloud N100, N50 and CCNC (0.6 %) are estimated at 24, 44 and 24 cm^{-3} for the upper cloud layer, 32, 52 and 32 cm^{-3} for the middle layer and 34, and 66 and 35 cm^{-3} for the lower layer. Comparison of the CCNC (0.6 %), which are in approximately the same concentration as the N100, and CDNC suggests S near or in excess of 0.6 %.

2.4.2 Low-altitude examples

5 and 7 July cases

The two examples in Fig. 4 are for cloud or fog over the polynyas north of Resolute Bay on 5 and 7 July. Four cloud samples were collected on 5 July at altitudes below 200 m. The time series in Fig. 4a covers the period of collection of the two lowest samples: 16:18:02–16:21:57 UT at 130 m and 16:39:35–16:40:18 UT at 88 m. In the air upwind of the cloud or fog, the N100, N30 and CCNC (0.6 %) are estimated at 3, 10–14 and 5 cm^{-3} . The mean values of the CDNC of 2.8 cm^{-3} at 130 m and 0.7 cm^{-3} at 88 m are explained by

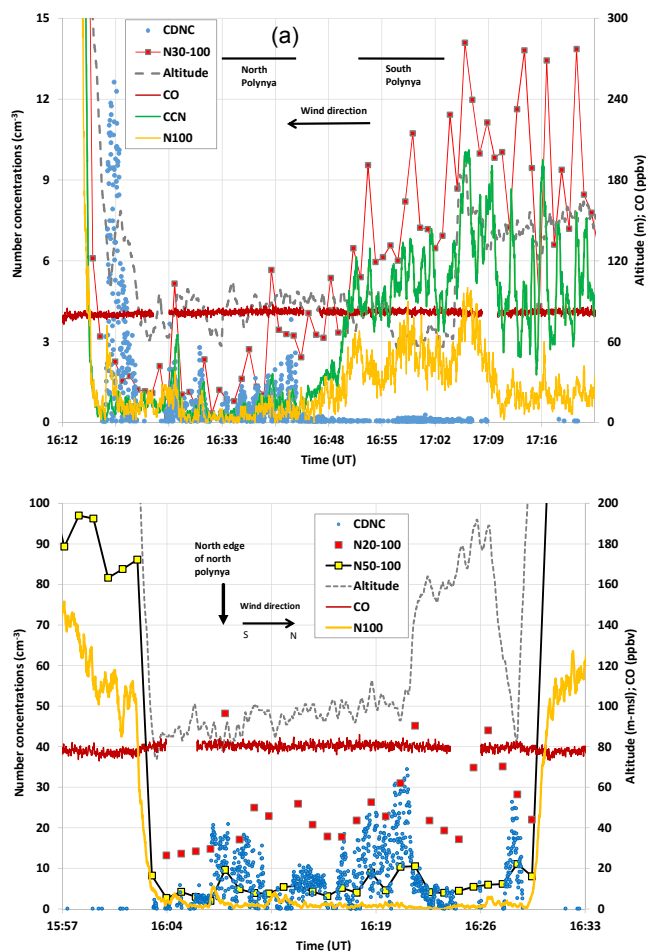


Figure 4. Time series during the sampling of low-altitude (LA) cloud or fog over the polynyas north of Resolute Bay. **(a)** 5 July time series showing CO, CDNC, CCNC (0.6 %) and particle number concentrations, where N30-100 is for particles sized between 30 and 100 nm and N100 is for particles sized > 100 nm. **(b)** 7 July time series showing CO, CDNC and particle number concentrations, where N20-100, N50-100 and N100 are for particles sized between 20 and 100 nm, between 50 and 100 and > 100 nm, respectively. CCNC (0.6 %) measurements are unavailable for this period on 7 July. Wind direction and relative position of polynyas are indicated in both panels. CDNC are referenced to STP.

the N100 and S less than 0.6 %. The maximum CDNC of 12 cm^{-3} at 130 m suggests the activation of smaller particles, possibly as small as 30 nm, and S exceeding 0.6 % perhaps due to some uplift influenced by orographic features north of the north polynya. At 88 m, the mean VMD (not shown) was $29 \mu\text{m}$ and ranged up to $35 \mu\text{m}$ giving those droplets potential to deposit over an hour or more, thereby potentially transferring water from the polynya to the downwind ice. On 7 July, cloud or fog was present below 120 m and thicker towards the north edge of the north polynya and again to the north over the ice. Seven samples were identified over the period 16:06–16:29 based on the LWC above 0.01 g m^{-3} .

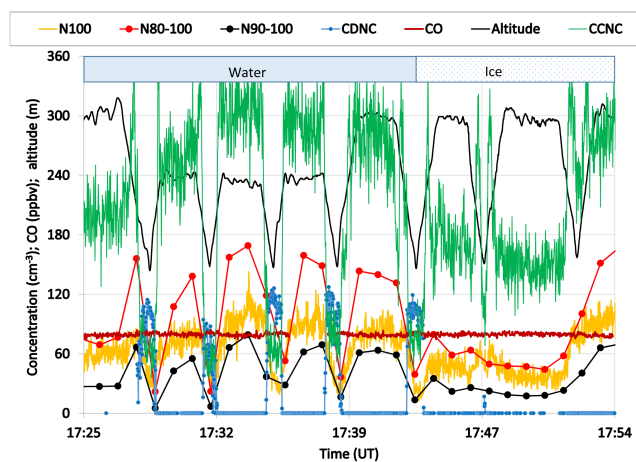


Figure 5. Time series of altitude, CO, N80-100, N90-100, N100, CCNC (0.6 %) and CDNC from low-altitude (LA) cloud sampling over Lancaster Sound on 8 July. The cloud was deeper over the open water of the Sound (see satellite picture in Fig. 2b). Over the ice to the west, the cloud was not as deep and could not be sampled. Segments over water and ice are indicated at the top of the figure.

The CDNC are overall higher than on 5 July with sample averages ranging from 4 to 13 cm^{-3} ; the 1 s CDNC are as high as 34 cm^{-3} and the mean VMDs (not shown) range from 19.6 to $22.8 \mu\text{m}$. The CO mixing ratio is slightly higher within the cloud (81 ppbv) than above (79 ppbv), although this difference may not be significant. In the air nearly free of cloud and below 120 m, the N100 is $4\text{--}5 \text{ cm}^{-3}$, the N50 is $8\text{--}11 \text{ cm}^{-3}$ and the N20 is variable between 17 and 130 cm^{-3} ; CCN are unavailable for this part of the flight. Mean values of CDNC/N100 and CDNC/N50 for seven cloud samples are 4.8 and 1.0, respectively, indicating that on average particles of about 50 nm were activated in this LA cloud. Based on the overall relationship between CCNC (0.6 %) and N50, which is discussed in Sect. 3.3, the mean S in the LA cloud of 7 July is estimated at 0.6 %. Comparison with the maximum CDNC suggests that particles as small as 20 nm may have participated in the nucleation of droplets.

8 July case

Figure 5 shows a time series of altitude, CO, N100, N80-100, N90-100, CCNC (0.6 %) and CDNC from the sampling above and in the low cloud over Lancaster Sound on 8 July. The cloud over the open water of the Sound is visible in the satellite picture in Fig. 2b. Cloud was also present over the ice to the west, but it was much thinner and reached only to about 150 m above the surface. Over the water, the cloud was sampled as high as 230 m by descending into it down to about 150 m between 17:27 and 17:43 UT as shown in Fig. 5. Observations in profiles from two of five samples are shown in Fig. 6. This cloud deepened as the aircraft approached the ice edge from over the water and thinned abruptly over the ice

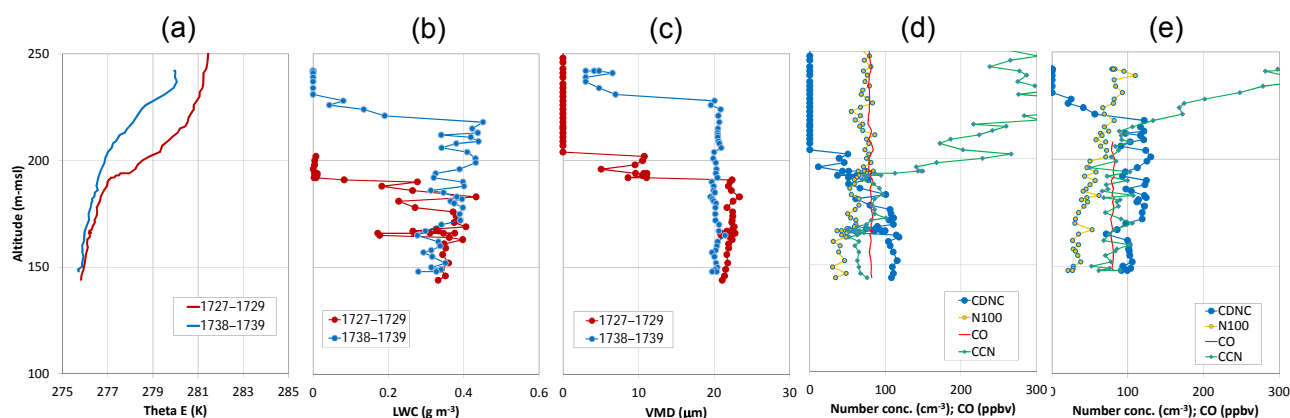


Figure 6. Profiles down into cloud showing (a) θ_e , (b) LWC and (c) VMD data for periods 17:27–17:29 and 17:38–17:39 UT on 8 July. (d) CDNC, N100, CO and CCNC (0.6 %) for the 17:27–17:29 UT profile. (e) CDNC, N100, CO and CCNC (0.6 %) for the 17:38–17:39 UT profile.

with tops below 150 m, as shown in Fig. 5 (time 17:47 UT). The thicker cloud was associated with a shift in wind direction to more southerly suggesting an influence of the Prince Regent Inlet and surrounding terrain on the flow as well as possibly circulations influenced by the water–ice transition. The cloud layer was relatively stable and the θ_e profiles suggest a surface heat sink (Fig. 6a). Profiles of LWC and VMD in Fig. 6b and c do not show increases with altitude characteristic of vertical mixing, such as for some of the HA clouds (Fig. 3); the change in the VMD per 50 m increase in height is about $1.7 \mu\text{m}$ for the well-mixed cloud of 7 July (Fig. 3a, b), whereas it is about $0.2 \mu\text{m}$ per 50 m for the LA cloud of flight 8 in Fig. 6. The CO mixing ratio shows little variation with time and altitude. The pre-cloud aerosol concentrations are more difficult to assess. Based on concentrations just above the cloud, particles $>90 \text{ nm}$ explain the CDNC. Based on concentrations downwind at 150 m (approximately 17:47 UT), activation of particles $>80 \text{ nm}$ is needed to explain the CDNC. The CCNC (0.6 %) are about 129 cm^{-3} downwind and between 157 and 234 cm^{-3} just above cloud. It is concluded that in this case the droplets likely nucleated on particles mostly larger than $80\text{--}95 \text{ nm}$ and the S in the clouds was less than 0.6 %. For the purposes of summary statistics discussed next, the N100, N50 and CCNC (0.6 %) have been selected as an average of the downwind and immediately above-cloud concentrations: 73 , 319 and 168 cm^{-3} , respectively.

3 Summary observations and discussion

Summary statistics for the cloud and aerosol samples are discussed in Sect. 3.1, the microphysics of low-altitude and higher-altitude clouds are contrasted in Sect. 3.2, particle activation is summarized in Sect. 3.3 and in Sect. 3.4 the relationship between VMD and CDNC is used to consider the transition of aerosol indirect effects from potential warming

to potential cooling. All analyses are based on the 62 cloud samples discussed in Sect. 2.4. The LA cloud subset is comprised of 24 samples and the HA cloud subset consists of 38 samples.

3.1 Summary of mean observations

The mean and median values of the microphysical properties of the cloud and pre-cloud aerosols as well as the altitudes and temperatures derived from the 62 cloud samples are given in Table 1, separated between periods 1 and 2. Values of the CDNC and the LWC are given relative to in situ volumes as well as STP. As discussed above, the pre-cloud CCNC (0.6 %), N50 and N100 are averages of those values collected within about 50 m of cloud base where a cloud base was clear and achievable. In other cases the pre-cloud CCNC (0.6 %), N50 and N100 are the values at the similar or lower altitudes in the clear air upwind of the cloud, except in the case of 8 July when the pre-cloud aerosol is based on the measurements in the area downwind plus those immediately above cloud. The CCNC (0.6 %) samples in Table 1 are limited to 44 due to instrument problems, all of which occurred during the early part of 7 July.

Cloud liquid water paths (LWPs) are estimated for 36 of the samples when a complete profile between cloud base and cloud top was possible. The LWPs are shown at the bottom of Table 1. Of the 36 LWP estimates, 34 are above 200 m, and the mean and median altitudes are 1044 and 862 m, respectively. Not included in the summary statistics are the samples from 8 July shown in Figs. 5 and 6. For the minimum altitude reached in that cloud, the LWP ranged from 12 to 25 and thus the total LWP for that cloud exceeded 25.

During period 1, the median sampling altitude is lower and the temperatures are slightly below freezing compared with just above freezing during period 2. The CO mixing ratios are overall low and at approximately background values dur-

Table 2. Summary of averaged observations for low-altitude (LA) and higher-altitude (HA) clouds. Values without parentheses are referenced to ambient volumes and values in parentheses are referenced to STP. 5 and 95 are the 5th and 95th percentiles.

Measurement	LA (<200 m): 24 samples; 0.89 h in cloud			HA (>200 m): 38 samples; 0.72 h in cloud		
	Mean	Median	5; 95	Mean	Median	5; 95
Altitude (m m.s.l.)	129	127	79; 178	1485	1481	457; 2391
Temperature (°C)	+0.6	+0.2	−2.5; 2.9	−1.2	+0.9	−6.5; 2.7
CDNC (STP; cm ^{−3})	31 (30)	11 (10)	1;106 (1; 102)	101 (118)	91 (101)	28;211 (31; 245)
LWC (STP; g m ^{−3})	0.10 (0.10)	0.05 (0.05)	0.01; 0.34 (0.01; 0.33)	0.13 (0.15)	0.13 (0.15)	0.04; 0.25 (0.04; 0.30)
VMD (μm)	20.7	20.1	14.6; 31	13.4	12.5	9.1; 19.4
CCNC (0.6 %) (cm ^{−3}); (16 LA; 28 HA)	74	24	2; 184	90	58	21; 217
N50 (cm ^{−3})	91	11	4.2; 319	136	133	41; 334
N100 (cm ^{−3})	26	4	1.3; 73	73	47	20; 232
CDNC (STP)/CCNC (0.6 %)	0.61	0.57	0.18; 1.3	1.2	1.2	0.6; 1.9
CDNC (STP)/N50	0.61	0.44	0.14; 1.5	0.91	0.93	0.5; 1.3
CDNC (STP)/N100	2.3	1.4	0.35; 9.0	2.1	1.9	0.7; 3.7
CCNC (0.6 %)/N50	0.66	0.71	0.52; 0.7	0.68	0.64	0.5; 0.9
CCNC (0.6 %)/N100	1.8	1.6	0.96; 2.6	1.5	1.1	0.8; 3.4
CO (ppbv)	81	80	78; 82	86	83	77; 107

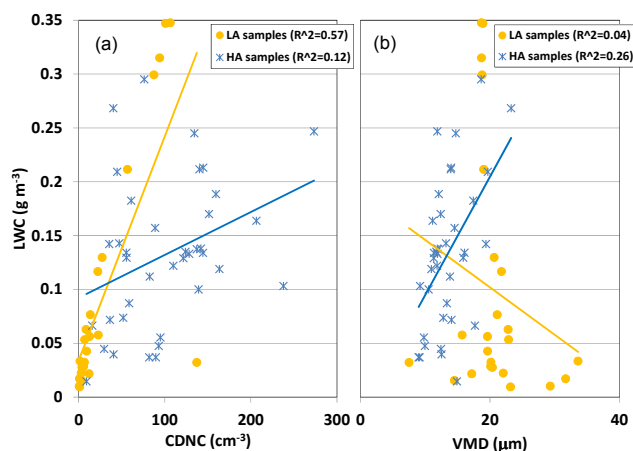


Figure 7. The LWC plotted as a function of the CDNC (a) and VMD (b) for the LA (orange) and HA (blue) samples. Linear regressions for each of the LA and HA samples are also plotted, and the coefficients of determination are given in the legends.

ing period 1. The median CDNC are higher during period 1 than period 2, but the mean values are similar. The CDNC compare more closely with the N50 during period 1, while during period 2 the CDNC are about equally between the N50 and N100. The CCNC (0.6 %) equated with particles between 50 and 100 nm during period 1, whereas during period 2 they were closer to the N100 values. The reduction in particle hygroscopicity during period 2 may be due to an increased presence of organics in the aerosol during that time (Willis et al., 2016).

3.2 Comparison of LA and HA cloud

The LA clouds were close to the surface, and all were associated with open water; some or all may be technically fogs. They may be formed by advection of warmer moist air over a cooler surface (the 8 July LA cloud that moved from Baffin Bay westward along Lancaster Sound was likely dominated by that process), by radiation cooling or by the passage of very cold air over a warm moist surface. The latter, also known as sea smoke, is the likely explanation for the clouds over the polynyas; also, it is possible that there was an advection component associated with the sea smoke moving from the polynyas over the ice surfaces. In general, the LA clouds are associated with low-level horizontal advection and heat and water exchange with the underlying ice or water surface. In contrast, vertical motions are responsible for some of the HA clouds, and none of the HA clouds interact so closely with the underlying surface. Due to those differences, the characteristics of the LA and HA clouds are considered separately. Table 2 shows the mean and median values for the samples separated between LA and HA clouds; vertical profiles of CDNC, LWC and VMD samples are shown in Fig. S7. On average, the LA samples have lower CDNC and higher VMD compared with the HA cases, and the LA clouds are activating on larger particles relative to the HA clouds (e.g. CDNC/N50). The values of the CDNC/CCNC (0.6 %) indicate that the *S* is <0.6 % for the LA clouds and close to 0.6 % for the HA clouds.

Variations in LWC are correlated with those of CDNC for the LA samples (Fig. 7a). The coefficient of determination (R^2) rises from 0.57 to 0.98 if the one LA point at

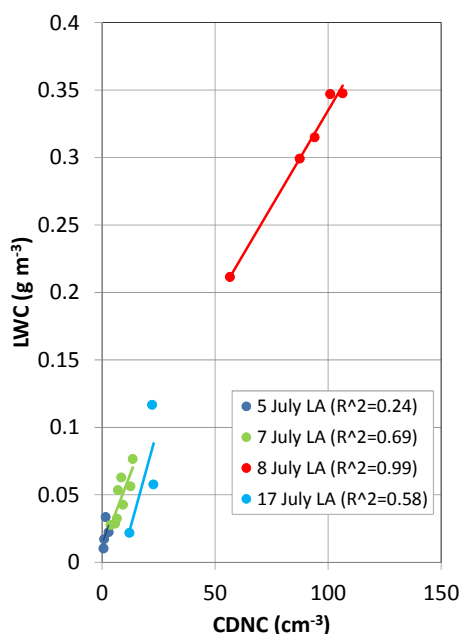


Figure 8. As in Fig. 7a, but identifying the specific LA cases of 5, 7, 8 and 17 July. Linear regressions for each set of samples are also plotted, and the coefficients of determination are given in the legends. The slopes are significant at a 95 % confidence level within ± 30 % for 7 July and within 60 % for 8 July. The slopes in the 5 and 17 July cases are not significant at a 95 % confidence level.

(137, 0.032) is removed. In contrast, the correlation of the LWC with the CDNC for the HA samples is low ($R^2 = 0.12$). There is no correlation of the LWC with the VMD for the LA points ($R^2 = 0.04$), and for the HA clouds there is a modest correlation of LWC with MVD ($R^2 = 0.26$). Variations in LWC with VMD within a cloud system are consistent with lifting of air from below, i.e. nucleation of droplets at cloud base followed by their growth with increasing altitude, such as the case shown in Fig. 3a and b. Variations of LWC with VMD can also result from homogeneous mixing (i.e. entrainment of dry air that reduces LWC by partial evaporation of droplets without reducing CDNC). The strong dependence of the variations in LWC with those of the CDNC in the LA clouds may reflect changes in rate of cooling, collision–coalescence or inhomogeneous mixing along the cloud transport pathway. For example, increases in the rate of cooling within or between clouds will increase condensation rates, and potentially S , resulting in increased LWC and CDNC. Changes in collision–coalescence will affect the CDNC and LWC in similar ways: more collision–coalescence, lower CDNC and lower LWC due to precipitation. Inhomogeneous mixing, the entrainment of dry air parcels into a cloud without mixing with the cloud droplets, will reduce the CDNC averaged across the cloud and at the same time reduce the mean LWC. Changes in the aerosol that are interactive with some of the cloud processes may con-

tribute to the CDNC and potentially the LWC through their influence on collision–coalescence.

The LWC–CDNC correlation is identifiable for individual flights with sufficient LA samples: four flights, comprising 20 of the 24 LA samples, had three or more points as shown in Fig. 8. The regressions for each of the 7, 8 and 17 July cases are approximately linear, and the respective mean VMDs are 20.8, 18.8 and 18.2 μm . The mean LWCs are 0.05, 0.3 and 0.07 g m^{-3} . The VMDs are relatively close together confirming similarities in the relationships, even if not purely linear. For comparison, the mean VMD for the 5 July samples is 29.2 μm and the LWC is 0.02 g m^{-3} , which indicates that the 5 July case does not fit the linear relationship shown in Fig. 8. The reasons behind the similarity of the VMD for the 7, 8 and 17 July are unknown, but it occurs despite the varied pre-cloud N50 and N100: N50 ranges from 5 to 272 cm^{-3} ; N100 ranges from 1.1 to 73 cm^{-3} . The consistencies among the three flights for greatly differing aerosol and CDNC imply a much smaller role for the aerosol in terms of the LWC. The distributions of droplets extend above 20 μm in these cases, but few are of sufficient size to initiate collision–coalescence (about 30 μm ; e.g. Rosenfeld et al., 2001) unless some fall out already had occurred. Greater temporal and spatial coverage is needed to assess the microphysical processes in these clouds.

3.3 Particle activation sizes

Here, the sizes and CCN activity of particles that acted as nuclei for cloud droplets are examined. The CDNC are plotted vs. N100 in Fig. 9a, separated between LA and HA samples. The CDNC are most often higher than the N100 and more so for the HA samples, which indicates that particles smaller than 100 nm activated in most cases and most often in the HA clouds. The mean and median values of CDNC(STP)/N100 are 2.2 and 1.8 for all 62 samples, and the 30th percentile of the CDNC/N100 is 1.2, which means that in about 70 % of the cases droplets nucleated on particles significantly smaller than 100 nm. Figure 9a can be compared with the results of Hegg et al. (2012), who showed a linear fit of CDNC to N100 for marine stratocumulus with a slope of 0.72 for which the N100 in 94 % of the samples was $> 150 \text{ cm}^{-3}$. Here, the slope is larger than unity is indicated, and the N100 is $< 100 \text{ cm}^{-3}$ in 90 % of the samples. The comparison indicates that relationships derived for higher-concentration environments do not necessarily apply to those of lower-concentration environments. In the clean environment often found in the Arctic during summer, the absence of larger particles may lower water uptake rates during droplet nucleation, which will increase S , enabling cloud droplets to nucleate on smaller particles; the absence of larger particles may also help increase the concentrations of smaller particles in the Arctic during summer by promoting new particle formation through a reduced condensation sink (e.g. Tunved et al., 2013; Leitch et al., 2013). The CDNC are plotted against the N50 in Fig. 9b,

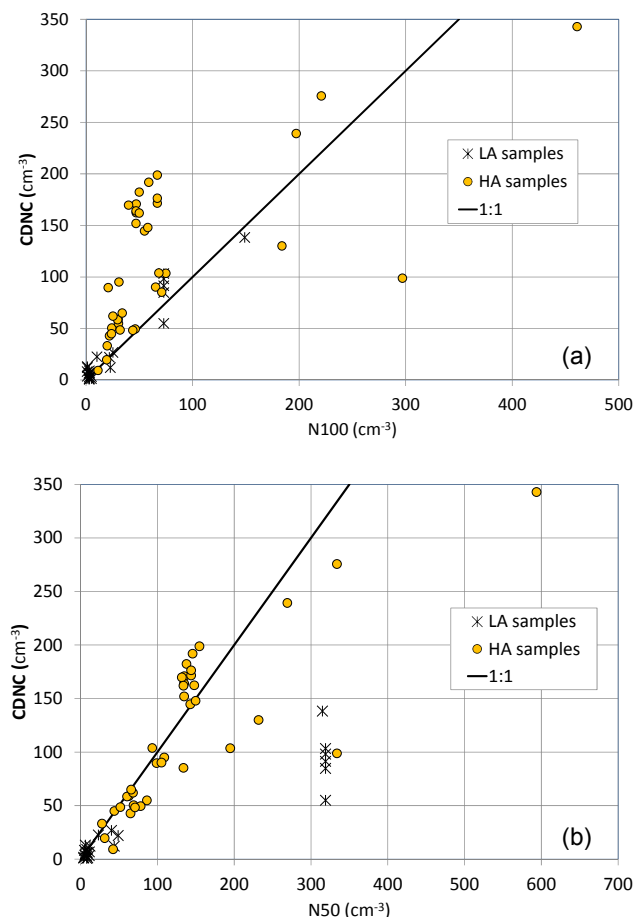


Figure 9. Plots of CDNC vs. (a) N100 and (b) N50. Points are identified between LA (yellow) and HA (black asterisk) samples, and the 1 : 1 lines are for reference.

showing that the mean activation size of the HA clouds was often close to 50 nm. The median value of CDNC/N50 is 0.78 for all samples indicating that, based on the averaged CDNC, cloud droplets nucleated on particles near or smaller than 50 nm about 40 % of the time. That percentage will increase if particle activation is considered relative to the maximum CDNC.

The mean and median values of the CCNC (0.6 %) associated with all cloud samples (84 and 47 cm⁻³) are generally consistent with previous Arctic CCNC measurements. For example, during the summer above 85° N, Martin et al. (2011) measured a mean CCNC at 0.73 % *S* of 47 cm⁻³ with a standard deviation of 35 cm⁻³, Yum and Hudson (2001) measured CCNC at 0.8 % *S* below 1700 m over the Beaufort Sea during May 1998 that ranged from 41 to 290 cm⁻³, and Radke et al. (1976) measured a mean CCNC at 1 % *S* of 90 cm⁻³ in June near Barrow, Alaska. Considering the median values of CDNC/CCNC (0.6 %) for the LA and HA samples (Table 2) and the slopes of linear regressions of CDNC vs. CCNC (0.6 %; Fig. 10a), the average

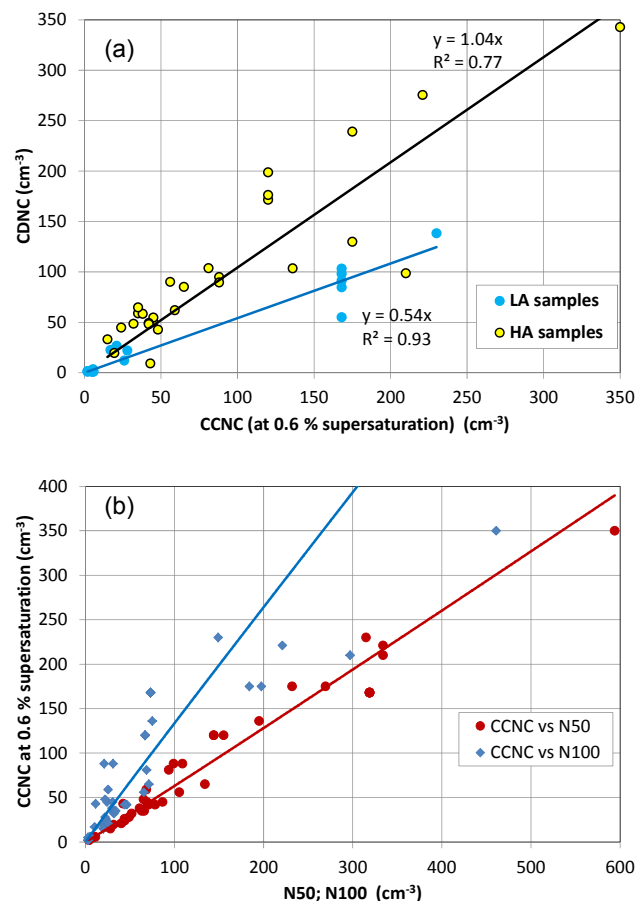


Figure 10. (a) CDNC plotted vs. the CCNC measured at 0.6 % supersaturation; points are identified between LA (yellow) and HA (blue) samples, and linear regressions through the origin are shown; the CCNC (0.6 %) points are limited to 44 of the 62 total due to problems with the CCN measurement; the 44 are split 16 and 28 between LA and HA. (b) CCNC (0.6 %; 44 points) plotted vs. N50 and N100; power-law fits to each are provided for reference.

inferred *S* for the HA clouds is about 0.6 %, consistent with the overall activation of smaller particles in those clouds. The mean *S* inferred for the LA clouds is significantly lower than 0.6 %. Based on the activation of a 90 nm particle (8 July case; CCNC (0.6 %) of 168 cm⁻³ in Fig. 10a) of low-moderate hygroscopicity, a reasonable estimate is 0.3 % for the mean of the LA clouds with some higher values indicated by the points near a CCNC (0.6 %) of 25 cm⁻³ in Fig. 10a. The *S* for these clean clouds is in contrast to polluted marine environments for which estimates for these types of clouds are 0.2 % or less (e.g. Modini et al., 2015). Consistent with the present results, Hudson et al. (2010) found that effective *S* in marine stratus tended to increase with a decrease in the CCNC, and for CCNC smaller than about 200 cm⁻³ their effective *S* ranged between 0.3 and 1.2 %.

Variations in the measured CCNC (0.6 %) are explained well by variations in smaller (N50) and larger (N100) parti-

cles as shown in Fig. 10b. The slopes of the power-law fits, for which the exponents are both close to unity, indicate that the CCNC (0.6 %) at 0.6 % S on average fall between 50 and 100 nm.

3.4 Aerosol influences on warming to cooling

The relationship between the VMD and CDNC shown in Fig. 11 exhibits a scattered but clear tendency for smaller VMD with increasing CDNC. The solid black curve is a reference line based on the study-mean LWC of 0.12 g m^{-3} (Table 1); points falling above or below the black curve have higher or lower LWC, respectively. The vertical dashed green line represents our best estimate of the Mauritsen limit below which Mauritsen et al. (2011) showed the cloud may produce a net warming for an increase in the CDNC. The net warming is a consequence of an increase in long-wave absorption due to an increase in the LWC, where the latter results from a reduction in deposition for the smaller droplets associated with increased CDNC. A value of 16 cm^{-3} is our best estimate of the Mauritsen limit for this data set because all points with CDNC below that value fall well below the mean LWC, therefore offering greater potential for changes in the CDNC to increase the LWC. Above the estimated Mauritsen limit, an increase in CDNC may produce a net cooling due to the cloud albedo effect, since at that point the long-wave forcing does not change significantly as the effects of deposition are minimized and the cloud effectively behaves as a black body.

The aerosol influence on clouds with CDNC below the Mauritsen limit is considered in Sect. 3.5. In Sect. 3.5, the potential background influence of the aerosol on clouds with CDNC above the Mauritsen limit is examined.

3.5 Below the Mauritsen limit

Seventeen of the 62 samples fall at or below our best estimate of the Mauritsen limit. Fifteen of those 17 samples are from LA clouds with median pre-cloud N50 and N100 estimates of 8.2 and 3.0 cm^{-3} , respectively. The lower number concentrations contribute to overall larger VMDs, although some of the points below the estimated Mauritsen limit have VMD values much less than $20 \mu\text{m}$. Increases in small particles, potentially from particle nucleation or fragmentation (e.g. Leck and Bigg, 1999, 2010), are hypothesized to increase the CDNC, thereby enhancing long-wave warming by these clouds, at least until the CDNC exceed the estimated Mauritsen limit. The LA points from the 5 July and 7 July cases, identified in Fig. 11, offer one insight. The median CDNC for 5 July is 6 times lower than the 7 July CDNC: 1.3 and 7.8 cm^{-3} for 5 and 7 July, respectively. The median N50 are 6 and 8.3 cm^{-3} for 5 and 7 July, respectively, and the median N100 is 3 and 2.2 cm^{-3} for 5 and 7 July, respectively. The CDNC are similar to N50 in the 7 July case, but lower than both the N50 and N100 in the 5 July case, indicating that the aerosol was not a limiting factor in the 5 July case. Consis-

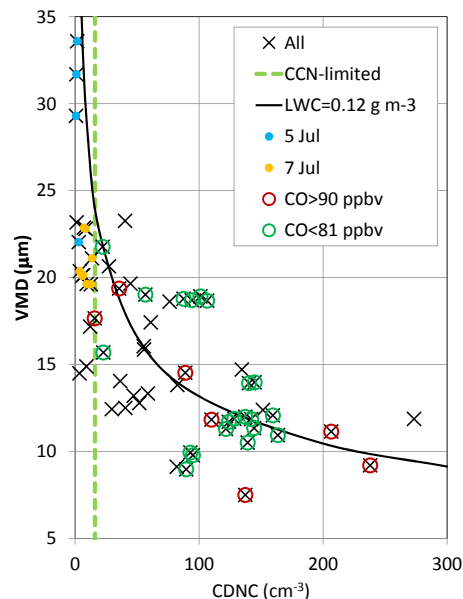


Figure 11. The mean VMD of all cloud samples plotted vs. the CDNC. All CDNC are referenced to the ambient pressure. The dashed vertical green line represents the “CCN-limited” division discussed by Mauritsen et al. (2011) and estimated here as 16 cm^{-3} . The solid black line is another reference showing the relationship between VMD and CDNC for a constant LWC: the study mean LWC of 0.12 g m^{-3} (Table 1). Samples with higher CO (> 90 ppbv) are identified by the open red circles, and samples with lower CO (< 81 ppbv) are identified by open green circles. Also highlighted for the discussion are LA samples from 5 July (blue dots) and 7 July (orange dots).

tent with the discussion in Sect. 3.2, all 15 LA points show a correlation of LWC with the CDNC ($R^2 = 0.57$), but correlations of CDNC with N50 and N100 are weak: $R^2 = 0.19$ and 0.06 , respectively. The CCN are not used here because only seven points with CCNC (0.6 %) are available; the seven do, however, correlate well with the N50. If the limit of 10 cm^{-3} of Mauritsen et al. (2011) is applied, reducing the number of points to 12, the assessment does not change: the LWC–CDNC correlation improves slightly and the correlations of the CDNC with the N100 and the N50 weaken.

The LWCs do not correlate with either the N50 or the N100 (Fig. S8). In this low CDNC environment, where cloud droplets may grow large enough to be gravitationally removed from the cloud without the support of collision–coalescence, the absence of a positive correlation of either the CDNC or LWC with the aerosol indicates that small changes in the aerosol did not contribute significantly to the changes in the LWC. Variations in other processes, such as mixing or the rate of cooling, may be responsible for the correlation of CDNC and LWC. It can be argued that some aerosol must exist for these clouds to form, but these observations show no association of changes in either the CDNC or LWC with changes in the aerosol.

3.6 Background aerosol influence on clouds

Above the estimated Mauritsen limit, the general reduction in the VMD with the CCNC-associated (0.6 %) increase in CDNC reflects the impact of increases in aerosol on clouds. In Fig. 11, samples are identified between those associated with lower CO (green circles; <81 ppbv, the median CO value of all samples) and those with highest CO (red circles; >90 ppbv); six samples have no CO measurement and the remaining points have CO falling within 81–90 ppbv. Five of the seven higher-CO samples are from the 19 July case (e.g. Fig. 3e, f) that has been linked with BB (Köllner et al., 2015), and the highest CDNC point (273 cm^{-3} ; no CO measurement) is also from 19 July and likely influenced by BB. The higher-CO samples cover a range of CDNC from 16 cm^{-3} to at least 238 cm^{-3} , with CO reaching up to 113 ppbv. The higher-CO samples are associated with larger particles ($N_{50}/N_{100} = 1.5$), consistent with a BB influence, compared with the lower-CO samples ($N_{50}/N_{100} = 3.2$). These values for BB fall at the low end of the observations from Zamora et al. (2016), but their CO concentrations are much higher than those measured in this study. The lower-CO samples may be dominated by regional biogenic emissions (Willis et al., 2016). The lower- and higher-CO points overlap over a CDNC range of 16 to 160 cm^{-3} , consistent with the range of pre-industrial CDNC from global models of 30 to 140 cm^{-3} (Penner et al., 2006; Korhonen et al., 2008). In this clean environment, the contributions from 20 to 100 nm particles have a broad impact on the range of CDNC, affirming the large uncertainty associated with estimating a baseline for the cloud albedo effect discussed by Carslaw et al. (2013).

4 Summary and conclusions

Aerosol particle size distributions, CCNC at 0.6 % water S , CO and cloud microphysics were measured from an airborne platform based out of Resolute Bay, Nunavut, from 4 to 21 July 2014 as one part of the Canadian NETCARE project. The flights were conducted over ice and water surfaces from about 60 m above the surface to about 6000 m. Sixty-two (62) cloud-averaged samples were derived, each constrained for the mean LWC > 0.01 g m^{-3} or the cloud threshold used here. The analysis separates the cloud samples between 24 low-altitude (<200 m) samples and 38 higher-altitude (>200 m) samples as well as situations of lower and higher CO and observations above and below the Mauritsen et al. (2011) CCNC (or CDNC) limit.

The median pre-cloud N_{100} of 33 cm^{-3} and the median CO mixing ratio of 81 ppbv indicate that the aerosols supporting the sampled clouds were relatively clean, and particularly during the first part of the study many of the aerosol particles may have been derived from regional natural sources. The median CDNC at STP is 10 cm^{-3} for the LA clouds (24 samples) and 101 cm^{-3} for the HA clouds (38 samples),

which correspond with the median pre-cloud N_{50} of 11 cm^{-3} for the LA samples and 133 cm^{-3} for the HA samples. The lower sizes of particles activated in cloud varied from about 20 to above 100 nm. In 40 % of cases, the average lower size of activation was 50 nm or smaller. Overall, smaller particles were activated more often in the HA clouds. Variations in particle chemistry will induce some variance in these results; however, because activation diameters are estimated starting with larger particles and moving to smaller sizes, changes in chemistry only offer the possibility of activation of particles still smaller than estimated here, which would have to occur at the expense of larger particles.

From the median values of CDNC/CCNC (0.6 %; 1.2 for the HA clouds and 0.6 for the LA clouds) and the linear regression of CDNC and CCNC (0.6 %), it is inferred that the average S was approximately 0.6 % for the HA clouds and 0.3 % for the LA clouds. Higher estimates will be obtained if the maximum CDNC are taken into consideration rather than the mean CDNC. The relatively high S for these clean Arctic stratus and stratocumulus has similarities with the observations of Hudson et al. (2010) for relatively clean stratus off the coast of California.

In 17 cases, 15 of which are LA clouds, the CDNC fell at or below the CCN limit discussed by Mauritsen et al. (2011), which is estimated here as 16 cm^{-3} . These are the first collection of simultaneous observations of the microphysics of aerosols and clouds in this unique regime in which the net radiative impact of increases in the CDNC is hypothesized to be warming due to changes in the LWC. The LWCs of the points below the Mauritsen limit all fall below the study-mean LWC, and the LWC increases with the CDNC. Neither the CDNC nor the LWC are positively correlated with the pre-cloud aerosol (N_{50} or N_{100}). In this environment of low cloud or fog and ultra-low CDNC, variations in cloud processes such as mixing or the rate of cooling may be responsible for the correlation of CDNC and LWC. These observations show no association of changes in either the CDNC or LWC with changes in the aerosol within the Mauritsen limit.

Forty-five cloud samples with CDNC above the Mauritsen limit exhibit a clear influence of changing aerosol. The cloud microphysics for the clouds formed in cleaner air (smaller particles and lower CO: <81 ppbv) overlap with clouds formed in what was likely more polluted air (larger particles and higher CO: >90 ppbv) covering a CDNC range of $16\text{--}160\text{ cm}^{-3}$. It is concluded that 20–100 nm particles from natural sources can have a broad impact on the range of CDNC in clean environments, affirming a large uncertainty in estimating a baseline for the cloud albedo effect.

5 Data availability

The complete data set is available from the NETCARE web site (www.netcare-project.ca) by contacting Richard Leaitch (richard.leaitch@ec.gc.ca) or Jon Abbatt

(jabbatt@chem.utoronto.ca). A table containing the details of the 62 samples discussed here is included with the Supplement.

The Supplement related to this article is available online at doi:10.5194/acp-16-11107-2016-supplement.

Acknowledgements. The authors acknowledge a large number of people for their contributions to this work. We thank Kenn Borek Air, in particular Kevin Elke and John Bayes, for their skillful piloting that facilitated these cloud observations. We are grateful to John Ford, David Heath and the U of Toronto machine shop, Jim Hodgson and Lake Central Air Services in Muskoka, Jim Watson (Scale Modelbuilders, Inc.), Julia Binder and Martin Gerhmann (AWI), Mike Harwood and Andrew Elford (EC) for their support of the integration of the instrumentation and aircraft. We thank Mohammed Wasey for his support of the instrumentation during the integration and in the field. We are grateful to Carrie Taylor (EC), Bob Christensen (U of T), Kevin Riehl (Kenn Borek Air), Lukas Kandora, Manuel Sellmann and Jens Herrmann (AWI), Desiree Toom, Sangeeta Sharma, Dan Veber, Andrew Platt, Anne Mari Macdonald, Ralf Staebler and Maurice Watt (EC), Kathy Law and Jennie Thomas (LATMOS) for their support of the study. We thank the biogeochemistry department of MPIC for providing the CO instrument and Dieter Scharffe for his support during the preparation phase of the campaign. We thank the Nunavut Research Institute and the Nunavut Impact Review Board for licensing the study. Logistical support in Resolute Bay was provided by the Polar Continental Shelf Project (PCSP) of Natural Resources Canada under PCSP Field Project no. 218-14, and we are particularly grateful to Tim McCagherty and Jodi MacGregor of the PCSP. Funding for this work was provided by the Natural Sciences and Engineering Research Council of Canada through the NETCARE project of the Climate Change and Atmospheric Research Program, the Alfred Wegener Institute and Environment and Climate Change Canada.

Edited by: V.-M. Kerminen

Reviewed by: J. Hudson and two anonymous referees

References

Aliabadi, A. A., Staebler, R. M., Liu, M., and Herber, A.: Characterization and Parametrization of Reynolds Stress and Turbulent Heat Flux in the Stably-Stratified Lower Arctic Troposphere Using Aircraft Measurements, *Bound.-Lay. Meteorol.*, doi:10.1007/s10546-016-0164-7, 2016a.

Aliabadi, A. A., Thomas, J. L., Herber, A. B., Staebler, R. M., Leaitch, W. R., Schulz, H., Law, K. S., Marelle, L., Burkart, J., Willis, M. D., Bozem, H., Hoor, P. M., Köllner, F., Schneider, J., Levasseur, M., and Abbatt, J. P. D.: Ship emissions measurement in the Arctic by plume intercepts of the Canadian Coast Guard icebreaker Amundsen from the Polar 6 aircraft platform, *Atmos. Chem. Phys.*, 16, 7899–7916, doi:10.5194/acp-16-7899-2016, 2016b.

Barrie, L. A.: Arctic air pollution: An overview of current knowledge, *Atmos. Environ.*, 20, 643–663, doi:10.1016/0004-6981(86)90180-0, 1986.

Barrie, L. A., Bottenheim, J. W., Schnell, R. C., Crutzen, P. J., and Rasmussen, R. A.: Ozone depletion and photochemical reactions at polar sunrise in the lower Arctic atmosphere, *Nature*, 334, 138–141, 1988.

Brenner, T. C., Curry, J. A., and Pinto, J. O.: Radiative transfer in the summertime Arctic, *J. Geophys. Res.*, 106, 15173–15183, 2001.

Brock, C. A., Cozic, J., Bahreini, R., Froyd, K. D., Middlebrook, A. M., McComiskey, A., Brioude, J., Cooper, O. R., Stohl, A., Aikin, K. C., de Gouw, J. A., Fahey, D. W., Ferrare, R. A., Gao, R.-S., Gore, W., Holloway, J. S., Hübler, G., Jefferson, A., Lack, D. A., Lance, S., Moore, R. H., Murphy, D. M., Nenes, A., Novelli, P. C., Nowak, J. B., Ogren, J. A., Peischl, J., Pierce, R. B., Pilewskie, P., Quinn, P. K., Ryerson, T. B., Schmidt, K. S., Schwarz, J. P., Sodemann, H., Spackman, J. R., Stark, H., Thomson, D. S., Thornberry, T., Veres, P., Watts, L. A., Warneke, C., and Wollny, A. G.: Characteristics, sources, and transport of aerosols measured in spring 2008 during the aerosol, radiation, and cloud processes affecting Arctic Climate (ARCPAC) Project, *Atmos. Chem. Phys.*, 11, 2423–2453, doi:10.5194/acp-11-2423-2011, 2011.

Browse, J., Carslaw, K. S., Mann, G. W., Birch, C. E., Arnold, S. R., and Leck, C.: The complex response of Arctic aerosol to sea-ice retreat, *Atmos. Chem. Phys.*, 14, 7543–7557, doi:10.5194/acp-14-7543-2014, 2014.

Cai, Y., Montague, D. C., Mooiweer-Bryan, W., and Deshler, T.: Performance characteristics of the ultra-high sensitivity aerosol spectrometer for particles between 55 and 800 nm: Laboratory and field studies, *J. Aerosol Sci.*, 39, 759–769, 2008.

Carslaw, K. S., Lee, L. A., Reddington, C. L., Pringle, K. J., Rap, A., Forster, P. M., Mann, G. W., Spracklen, D. V., Woodhouse, M. T., Regayre, L. A., and Pierce, J. R.: Large contribution of natural aerosols to uncertainty in indirect forcing, *Nature*, 503, 67–71, doi:10.1038/nature12674, 2013.

Christensen, J. H., Kanikicharla, K. K., Marshall, G., and Turner, J.: Chapter 14, in *Climate Change, 2013, The Physical Basis*, edited by: Stocker, T. F., Qin, D., Plattner, G.-K., Tignor, M. M. B., Allen, S. K., Boschung, J., Nauels, A., Xia, Y., Bex, V., and Midgley, P. M., Intergovernmental Panel on Climate Change, Cambridge University Press, Cambridge, UK, 1217–1308, 2013.

Curry, J. A.: Introduction to special section: FIRE Arctic clouds experiment, *J. Geophys. Res.*, 106, 14985–14987, 2001.

Earle, M. E., Liu, P. S. K., Strapp, J. W., Zelenyuk, A., Imre, D., McFarquhar, D. M., Shantz, N. C., and Leaitch, W. R.: Factors influencing the microphysics and radiative properties of liquid-dominated Arctic clouds: Insight from observations of aerosol and clouds during ISDAC (2008), *J. Geophys. Res.*, 116, D00T09, doi:10.1029/2011JD015887, 2011.

Engvall, A.-C., Krejci, R., Ström, J., Treffeisen, R., Scheele, R., Hermansen, O., and Paatero, J.: Changes in aerosol properties during spring-summer period in the Arctic troposphere, *Atmos. Chem. Phys.*, 8, 445–462, doi:10.5194/acp-8-445-2008, 2008.

Garrett, T. J., Zhao, C., Dong, X., Mace, G. G., and Hobbs, P. V.: Effects of varying aerosol regimes on low-level Arctic stratus, *Geophys. Res. Lett.*, 31, L17105, doi:10.1029/2004GL019928, 2004.

- Garrett, T. J., Maestas, M. M., Krueger, S. K., and Schmidt C. T.: Acceleration by aerosol of a radiative-thermodynamic cloud feedback influencing Arctic surface warming, *Geophys. Res. Lett.*, 36, L19804, doi:10.1029/2009GL040195, 2009.
- Hallett, J., and L. Christensen: The splashing and penetration of raindrops into water, *J. Rech. Atmos.* 18, 226–242, 1984.
- Heintzenberg, J. and Leck C.: Seasonal-variation of the atmospheric aerosol near the top of the marine boundary layer over Spitsbergen related to the Arctic sulphur cycle, *Tellus B*, 46, 52–67, doi:10.1034/j.1600-0889.1994.00005.x, 1994.
- Heintzenberg, J., Leck, C., Birmili, W., Wehner, B., Tjernström, M., and Wiedensohler, A.: Aerosol number-size distributions during clear and fog periods in the summer high Arctic: 1991, 1996, and 2001, *Tellus*, 58B, 41–50, 2006.
- Heintzenberg, J., Leck, C., and Tunved, P.: Potential source regions and processes of aerosol in the summer Arctic, *Atmos. Chem. Phys.*, 15, 6487–6502, doi:10.5194/acp-15-6487-2015, 2015.
- Hegg, D. A., Covert, D. S., Jonsson, H. H., and Woods, R. K.: A simple relationship between cloud drop number concentration and precursor aerosol concentration for the regions of Earth's large marine stratocumulus decks, *Atmos. Chem. Phys.*, 12, 1229–1238, doi:10.5194/acp-12-1229-2012, 2012.
- Herber, A., Dethloff, K., Haas, C., Steinhage, D., Strapp, J. W., Bottenheim, J., McElroy, T., and Yamanouchi, T.: POLAR 5 – a new research aircraft for improved access to the Arctic, ISAR-1, Drastic Change under the Global Warming, Extended Abstract, 54–57, 2008
- Herman, G. F.: Solar radiation in summertime Arctic stratus clouds, *J. Atmos. Sci.*, 34, 1423–1432, 1977.
- Hobbs, P. V. and Rango, A. L.: Microstructures of low and middle-level clouds over the Beaufort Sea, *Q. J. Roy. Meteor. Soc.*, 124, 2035–2071, 1998.
- Hudson, J. G. and Frisbie, P. R.: Cloud condensation nuclei near marine stratus, *J. Geophys. Res.*, 96, 20795–20808, 1991.
- Hudson, J. G.: Cloud condensation nuclei near marine cumulus, *J. Geophys. Res.*, 98, 2693–2702, 1993.
- Hudson, J. G., Noble, S., and Jha, V.: Stratus clouds, *Geophys. Res. Lett.*, 37, L21813, doi:10.1029/2010GL045197, 2010.
- Intrieri, J. M., Shupe, M. D., Uttal, T., and McCarty, B. J.: An annual cycle of Arctic cloud characteristics observed by radar and lidar at SHEBA, *J. Geophys. Res.*, 107, C108030, doi:10.1029/2000JC000423, 2002.
- Jacob, D. J., Crawford, J. H., Maring, H., Clarke, A. D., Dibb, J. E., Emmons, L. K., Ferrare, R. A., Hostetler, C. A., Russell, P. B., Singh, H. B., Thompson, A. M., Shaw, G. E., McCauley, E., Pederson, J. R., and Fisher, J. A.: The Arctic Research of the Composition of the Troposphere from Aircraft and Satellites (ARCTAS) mission: design, execution, and first results, *Atmos. Chem. Phys.*, 10, 5191–5212, doi:10.5194/acp-10-5191-2010, 2010.
- Jouan, C., Pelon, J., Girard, E., Ancellet, G., Blanchet, J. P., and Delanoë, J.: On the relationship between Arctic ice clouds and polluted air masses over the North Slope of Alaska in April 2008, *Atmos. Chem. Phys.*, 14, 1205–1224, doi:10.5194/acp-14-1205-2014, 2014.
- Klingebiel, M., de Lozar, A., Molleker, S., Weigel, R., Roth, A., Schmidt, L., Meyer, J., Ehrlich, A., Neuber, R., Wendisch, M., and Borrmann, S.: Arctic low-level boundary layer clouds: in situ measurements and simulations of mono- and bimodal super-cooled droplet size distributions at the top layer of liquid phase clouds, *Atmos. Chem. Phys.*, 15, 617–631, doi:10.5194/acp-15-617-2015, 2015.
- Köllner, F., Schneider, J., Bozem, H., Hoor, P., Willis, M., Burkart, J., Leaitch, R., Abbatt, J., Herber, A., and Borrmann, S.: Pollution in the summertime Canadian High Arctic observed during NETCARE 2014: Investigation of origin and composition, in *Geophysical Research Abstracts*, 17, EGU2015-5951, European Geophysical Union General Assembly 2015, Vienna, Austria, 2015.
- Korhonen, H., Carslaw, K. S., Spracklen, D. V., Ridley, D. A., and Ström, J.: A global model study of processes controlling aerosol size distributions in the Arctic spring and summer, *J. Geophys. Res.*, 113, D08211, doi:10.1029/2007JD009114, 2008.
- Korolev, A. V., Emery, E. F., Strapp, J. W., Cober, S. G., Isaac, G. A., Wasey, M., and Marcotte, D.: Small ice particles in tropospheric clouds: fact or artifact? Airborne icing instrumentation evaluation experiment, *B. Am. Meteorol. Soc.*, 92, 967–973, 2011.
- Lance, S., Shupe, M. D., Feingold, G., Brock, C. A., Cozic, J., Holloway, J. S., Moore, R. H., Nenes, A., Schwarz, J. P., Spackman, J. R., Froyd, K. D., Murphy, D. M., Brioude, J., Cooper, O. R., Stohl, A., and Burkhart, J. F.: Cloud condensation nuclei as a modulator of ice processes in Arctic mixed-phase clouds, *Atmos. Chem. Phys.*, 11, 8003–8015, doi:10.5194/acp-11-8003-2011, 2011.
- Law, K. S. and Stohl, A.: Arctic air pollution: origins and impacts, *Science*, 315, 1537–1540, 2007.
- Leaitch, W. R., Lohmann, U., Russell, L. M., Garrett, T., Shantz, N. C., Toom-Saunty, D., Strapp, J. W., Hayden, K. L., Marshall, J., Wolde, M., Worsnop, D. R., and Jayne, J. T.: Cloud albedo increase from carbonaceous aerosol, *Atmos. Chem. Phys.*, 10, 7669–7684, doi:10.5194/acp-10-7669-2010, 2010.
- Leaitch, W. R., Sharma, S., Huang, L., Macdonald, A. M., Toom-Saunty, D., Chivulescu, A., von Salzen, K., Pierce, J. R., Shantz, N. C., Bertram, A., Schroder, J., Norman, A.-L., and Chang R. Y.-W.: Dimethyl sulphide control of the clean summertime Arctic aerosol and cloud, *Elementa: Science of the Anthropocene*, 1, 000017, doi:10.12952/journal.elementa.000017, 2013.
- Leck C. and Bigg, E.K.: Aerosol production over remote marine areas – A new route, *Geophys. Res. Lett.*, 26, 3577–3580, 1999.
- Leck C. and Bigg, E. K.: New particle formation of marine biological origin, *Aerosol Sci. Technol.*, 44, 570–577, doi:10.1080/02786826.2010.481222, 2010.
- Lohmann, U., Humble, J., Leaitch, R., Isaac, G., and Gultepe, I.: Simulations of ice clouds during FIRE.ACE using the CCCMA single column model, *J. Geophys. Res.*, 106, 15123–15138, 2001.
- Lohmann, U. and Leck, C.: Importance of submicron surface active organic aerosols for pristine Arctic clouds, *Tellus B*, 57, 261–268, 2005.
- Lubin, D. and Vogelmann, A.M.: Observational quantification of a total aerosol indirect effect in the Arctic, *Tellus*, 62B, 181–189, doi:10.1111/j.1600-0889.2010.00460.x, 2010.
- Martin, M., Chang, R. Y.-W., Sierau, B., Sjogren, S., Swietlicki, E., Abbatt, J. P. D., Leck, C., and Lohmann, U.: Cloud condensation nuclei closure study on summer arctic aerosol, *Atmos. Chem. Phys.*, 11, 11335–11350, doi:10.5194/acp-11-11335-2011, 2011.
- Maslanik, J., Stroeve, J., Fowler, C., and Emery, W.: Distribution and trends in Arctic sea ice age through spring 2011, *Geophys. Res. Lett.*, 38, L13502, doi:10.1029/2011gl047735, 2011, 2011.

- Mauritsen, T., Sedlar, J., Tjernström, M., Leck, C., Martin, M., Shupe, M., Sjogren, S., Sierau, B., Persson, P. O. G., Brooks, I. M., and Swietlicki, E.: An Arctic CCN-limited cloud-aerosol regime, *Atmos. Chem. Phys.*, 11, 165–173, doi:10.5194/acp-11-165-2011, 2011.
- Modini, R. L., Frossard, A. A., Ahlm, L., Russell, L. M., Corrigan, C. E., Roberts, G. C., Hawkins, L. N., Schroder, J. C., Bertram, A. K., Zhao, R., Lee, A. K. Y., Abbatt, J. P. D., Lin, J., Nenes, A., Wang, Z., Wonaeschütz, A., Sorooshian, A., Noone, K. J., Jonsson, H., Seinfeld, J. H., Toom-Sauntry, D., Macdonald, A. M., and Leaitch W. R.: Primary marine aerosol-cloud interactions off the coast of California, *J. Geophys. Res. Atmos.*, 120, 4282–4303, doi:10.1002/2014JD022963, 2015.
- Morrison, H., de Boer, G., Feingold, G., Harrington, J., Shupe, M. D., and Sulia K.: Resilience of persistent Arctic mixed-phase clouds, *Nat. Geosci.*, 5, 11–17, doi:10.1038/ngeo1332, 2012.
- Najafi, M. R., Zwiers, F. W., and Gillett N. P.: Attribution of Arctic temperature change to greenhouse-gas and aerosol influences, *Nature Climate Change*, 2524, doi:10.1038/NCLIMATE2524, 2015.
- Peng, Y., Lohmann, U., Leaitch, R., Banic, C., and Couture, M.: The cloud albedo – cloud droplet effective radius relationship for clean and polluted clouds from RACE and FIRE.ACE, *J. Geophys. Res.*, 107, 4106, doi:10.1029/2000JD000281, 2002.
- Penner, J. E., Quaas, J., Storelvmo, T., Takemura, T., Boucher, O., Guo, H., Kirkevåg, A., Kristjánsson, J. E., and Seland, Ø.: Model intercomparison of indirect aerosol effects, *Atmos. Chem. Phys.*, 6, 3391–3405, doi:10.5194/acp-6-3391-2006, 2006.
- Quinn, P. K., Bates, T. S., Baum, E., Doubleday, N., Fiore, A. M., Flanner, M., Fridlind, A., Garrett, T. J., Koch, D., Menon, S., Shindell, D., Stohl, A., and Warren, S. G.: Short-lived pollutants in the Arctic: their climate impact and possible mitigation strategies, *Atmos. Chem. Phys.*, 8, 1723–1735, doi:10.5194/acp-8-1723-2008, 2008.
- Radke, L. F., Hobbs, P. V., and Pinnons, J. E.: Observations of cloud condensation nuclei, sodium-containing particles, ice nuclei and the light-scattering coefficient near Barrow, Alaska, *J. Appl. Meteorol.*, 15, 982–995, 1976.
- Sandvik, A., Biryulina, M., Kvamsto, N., Stamnes, J., and Stamnes, K.: Observed and simulated microphysical composition of Arctic clouds: Data properties and model validation, *J. Geophys. Res.*, 112, D05205, doi:10.1029/2006JD007351, 2007.
- Shindell, D. T., Chin, M., Dentener, F., Doherty, R. M., Faluvegi, G., Fiore, A. M., Hess, P., Koch, D. M., MacKenzie, I. A., Sander-son, M. G., Schultz, M. G., Schulz, M., Stevenson, D. S., Teich, H., Textor, C., Wild, O., Bergmann, D. J., Bey, I., Bian, H., Cuvelier, C., Duncan, B. N., Folberth, G., Horowitz, L. W., Jonson, J., Kaminski, J. W., Marmer, E., Park, R., Pringle, K. J., Schroeder, S., Szopa, S., Takemura, T., Zeng, G., Keating, T. J., and Zuber, A.: A multi-model assessment of pollution transport to the Arctic, *Atmos. Chem. Phys.*, 8, 5353–5372, doi:10.5194/acp-8-5353-2008, 2008.
- Shupe, M. D., Kollias, P., Matrosov, S. Y., and Schneider, T. L.: Deriving mixed-phase cloud properties from Doppler radar spectra, *J. Atmos. Ocean. Technol.*, 21, 660–670, 2004.
- Shupe, M. D., Persson, P. O. G., Brooks, I. M., Tjernström, M., Sedlar, J., Mauritsen, T., Sjogren, S., and Leck, C.: Cloud and boundary layer interactions over the Arctic sea ice in late summer, *Atmos. Chem. Phys.*, 13, 9379–9399, doi:10.5194/acp-13-9379-2013, 2013.
- Stohl A.: Characteristics of atmospheric transport into the Arctic troposphere, *J. Geophys. Res.*, 111, D11306, doi:10.1029/2005JD006888, 2006.
- Stohl, A., Klimont, Z., Eckhardt, S., Kupiainen, K., Shevchenko, V. P., Kopeikin, V. M., and Novigatsky, A. N.: Black carbon in the Arctic: the underestimated role of gas flaring and residential combustion emissions, *Atmos. Chem. Phys.*, 13, 8833–8855, doi:10.5194/acp-13-8833-2013, 2013.
- Ström, J., Umegård, J., Tørseth, K., Tunved, P., Hansson, H.-C., Holmém, K., Wismann, V., Herber, A., and König-Langlo, G.: One year of particle size distribution and aerosol chemical composition measurements at the Zeppelin Station, Svalbard, March 2000–March 2001, *Phys. Chem. Earth*, 28, 1181–1190, 2003.
- Tjernström, M., Leck, C., Persson, P. O. G., Jensen, M. L., Oncley, S. P., and Targino, A.: The summertime Arctic atmosphere: Meteorological measurements during the Arctic Ocean experiment 2001 (AOE-2001), *B. Am. Meteorol. Soc.*, 85, 1305–1321, 2004, 2004.
- Tjernström, M., Leck, C., Birch, C. E., Bottenheim, J. W., Brooks, B. J., Brooks, I. M., Bäcklin, L., Chang, R. Y.-W., de Leeuw, G., Di Liberto, L., de la Rosa, S., Granath, E., Graus, M., Hansel, A., Heintzenberg, J., Held, A., Hind, A., Johnston, P., Knulst, J., Martin, M., Matrai, P. A., Mauritsen, T., Müller, M., Norris, S. J., Orellana, M. V., Orsini, D. A., Paatero, J., Persson, P. O. G., Gao, Q., Rauschenberg, C., Ristovski, Z., Sedlar, J., Shupe, M. D., Sierau, B., Sirevaag, A., Sjogren, S., Stetzer, O., Swietlicki, E., Szczodrak, M., Vaattovaara, P., Wahlberg, N., Westberg, M., and Wheeler, C. R.: The Arctic Summer Cloud Ocean Study (ASCOS): overview and experimental design, *Atmos. Chem. Phys.*, 14, 2823–2869, doi:10.5194/acp-14-2823-2014, 2014.
- Tunved, P., Ström, J., and Krejci, R.: Arctic aerosol life cycle: linking aerosol size distributions observed between 2000 and 2010 with air mass transport and precipitation at Zeppelin station, Ny-Ålesund, Svalbard, *Atmos. Chem. Phys.*, 13, 3643–3660, doi:10.5194/acp-13-3643-2013, 2013.
- United Nations Environment Programme: Near-term Climate Protection and Clean Air Benefits: Actions for Controlling Short-Lived Climate Forcers, UNEP, Nairobi, Kenya, available at: <http://www.unep.org/publications/ebooks/SLCF/> (last access: 29 August 2016), 2011.
- Willis, M. D., Burkart, J., Thomas, J. L., Köllner, F., Schneider, J., Bozem, H., Hoor, P. M., Aliabadi, A. A., Schulz, H., Herber, A. B., Leaitch, W. R., and Abbatt, J. P. D.: Growth of nucleation mode particles in the summertime Arctic: a case study, *Atmos. Chem. Phys.*, 16, 7663–7679, doi:10.5194/acp-16-7663-2016, 2016.
- Wylie, D. and Hudson, J. G.: Effects of long range transport and clouds on cloud condensation nuclei in the Springtime Arctic, *J. Geophys. Res.*, 107, 4318, doi:10.1029/2001JD000759, 2002.
- Yum, S. S. and Hudson, J. G.: Vertical distributions of cloud condensation nuclei spectra over the springtime Arctic Ocean, *J. Geophys. Res.*, 106, 15045–15052, doi:10.1029/2000JD900357, 2001.

Zamora, L. M., Kahn, R. A., Cubison, M. J., Diskin, G. S., Jimenez, J. L., Kondo, Y., McFarquhar, G. M., Nenes, A., Thornhill, K. L., Wisthaler, A., Zelenyuk, A., and Ziemba, L. D.: Aircraft-measured indirect cloud effects from biomass burning smoke in the Arctic and subarctic, *Atmos. Chem. Phys.*, 16, 715–738, doi:10.5194/acp-16-715-2016, 2016.

Zhao, C. and Garrett, T. J.: Effects of Arctic haze on surface cloud radiative forcing, *Geophys. Res. Lett.*, 557–564, 10.1002/2014GL062015, 2015.